1 *Electronic Supplementary Information (ESI)*

2

3 **Intramolecular-locked Triphenylamine Derivatives with**

4 **Adjustable Room Temperature Phosphorescence Property**

5 **by Substituent Effect**

6 Mengmeng Han [a], Zhichen Xu [a], Jie Lu [a], Yujun Xie [b], Qianqian Li [a,*], Zhen Li [a,b,*]

7

8 [a] Hubei Key Lab on Organic and Polymeric Opto-Electronic Materials, Sauvage Center for

9 Molecular Sciences, Department of Chemistry, Wuhan University, Wuhan 430072, China.

10 [b] Institute of Molecular Aggregation Science, Tianjin University, Tianjin 300072, China.

11
12
13
14
15
16
17
18
19
20
21
22
23
24
25
26
27
28
29
30
31
32
33
34
35
36
37

1 **Table of content**

2 **Experimental section**

3 1. Experiment section

4 1.1. Materials

5   Toluene was dried by sodium-potassium alloy. All other chemicals reagents and solvents were obtained from

6 commercial sources and used as received without further purification.

7

8 1.2. Instruments

9   ^{1}H and ^{13}C NMR spectra were recorded on a Bruker Avance III HD 400 MHz using tetramethylsilane (TMS; δ

10 = 0 ppm) as internal standard. Elemental analyses were performed by a Perkin-Elmer microanalyzer. Mass spectra

11 were measured on a ZAB 3F-HF mass spectrophotometer. UV-vis spectra were conducted on a Shimadzu UV-2550

12 spectrometer. Fluorescence spectra and low temperature phosphorescence spectra were performed on a Hitachi

13 F-4600 fluorescence spectrophotometer. Photoluminescence spectra, quantum yields and lifetimes were

14 determined with FLS980 spectrometer. The powder X-ray diffraction patterns were recorded by D8 Advanced

15 (Bruker) using Cu-Kα radiation from 10 to 50°. The single-crystal X-ray diffraction data of C-TPA, C-TPA-Me and C-

16 TPA-OMe crystals were collected in a Bruker Smart Apex CCD diffractometer. The time-dependent

17 phosphorescence spectra were collected from an Ocean Optics QE65 Pro spectrometer. The single-crystal X-ray

18 diffraction data was collected in a Bruker Smart Apex CCD diffractometer.

19

20 1.3. Theoretical Calculation

21   TD-DFT calculations were performed on Gaussian 09 program [1]. The ground state (S_0) geometries were

22 optimized with the Becke's three-parameter exchange functional along with the Lee Yang Parr's correlation

23 functional (B3LYP) using 6-31G (d) basis sets. The excitation energies in the n-th singlet (S_n) and n-th triplet (T_n)

24 states of monomer and dimers were obtained using the TD-DFT method based on single crystal diffraction data at

25 ground state (S_0). The NTO analysis by using Multiwfn 3.8 software.[2]

26

27 **2 Synthetic procedures**

28 **2.1 Synthesis**

29
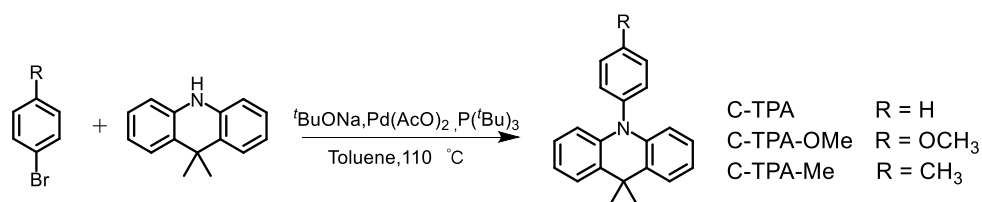
30   **Scheme S1.** The synthetic route of these three compounds C-TPA, C-TPA-OMe and C-TPA-Me.

31 **The general synthesis route of C-TPA, C-TPA-OMe and C-TPA-Me:**

32   A mixture of *p*-bromobenzene-derivatives (3.3 mmol, 1 equiv.), 9,9-dimethyl-9,10-dihydroacridine (3.0 mmol,

33 1.1 equiv.), palladium acetate (3% mol), tri-tert-butylphosphine (3.6% mol) and sodium tert-butoxide (3.6 mmol,

34 1.2 equiv.) in dry and degassed toluene (40 mL) was refluxed overnight at 110℃ and in N_2 atmosphere. After

35 cooling to room temperature, the reaction mixture was treated with brine and then extracted with

36 dichloromethane for three times. The organic layers were collected and combined. Then, the solvent was removed

37 by using rotary evaporators. The resulting product was purified by column chromatography on silica gel using

38 petroleum ether as eluent to desired materials as a light white solid.

39 **C-TPA:** white solid(yield :85%). mp: 114 ^{o}C; ^{1}H NMR (400 MHz, CDCl$_3$) δ 7.62 (d, *J* = 8.0 Hz, 2H, ArH), 7.47 (dd, *J* =

40 7.6, 1.6 Hz, 3H, ArH), 7.37 – 7.33 (m, Ar-H, 2H), 7.04 – 6.86 (m, 4H, ArH), 6.27 (dd, *J* = 8.0, 1.6 Hz, 2H, ArH), 1.71 (s,

6H, -CH$_3$); ^{13}C NMR (100 MHz, CDCl$_3$) δ 141.23, 140.96, 131.35, 130.86, 129.97, 128.22, 126.35, 125.20, 120.51, 114.04, 36.00, 31.26. MS (EI), m/z: 285.15 ([M]$^+$ calcd for C$_{21}$H$_{19}$N: 285.15); Anal. calcd for C$_{21}$H$_{19}$N: C, 88.38; H, 6.71; N, 4.91, Found: C, 88.08; H, 6.26; N, 4.84.

C-TPA-OMe: White solid (yield: 76%). mp: 152 ^{o}C; ^{1}H NMR (400 MHz, CDCl$_3$) δ 7.44 (dd, J = 7.6, 1.6 Hz, 2H, ArH), 7.25 − 7.21 (m, 2H, ArH), 7.14 − 7.09 (m, 2H, ArH), 6.94 (m,4H, ArH), 6.30 (dd, J = 8.0, 1.6 Hz, 2H, ArH), 3.91 (s, 3H, -CH$_3$), 1.68 (s, 6H, -CH$_3$); ^{13}C NMR (100 MHz, CDCl$_3$) δ 159.14, 141.26, 133.69, 132.20, 129.97, 126.33, 125.16, 120.39, 115.98, 114.02, 55.54, 35.96, 31.26; MS (EI), m/z: 315.15 ([M]$^+$ calcd for C$_{22}$H$_{21}$NO: 315.16); Anal. calcd for C$_{22}$H$_{21}$NO: C, 83.78; H, 6.71; N, 4.44; Found: C, 83.48; H, 6.25; N, 4.30.

C-TPA-Me: White solid (yield: 72%), mp: 150 ^{o}C; ^{1}H NMR (400 MHz, CDCl$_3$) δ 7.49 − 7.37 (m, 2H, ArH), 7.24 − 7.18 (m, 2H, ArH), 6.94 (m, 4H, ArH), 6.30 (dd, J = 8.0, 1.6 Hz, 2H, ArH), 2.49 (s, 3H, -CH$_3$), 1.69 (s, 6H, -CH$_3$); ^{13}C NMR (100 MHz, CDCl$_3$) δ 141.07, 138.44, 138.04, 131.51, 130.96, 129.94, 126.32, 125.16, 120.38, 114.05, 35.97, 31.27, 21.33; MS (EI), m/z: 299.15 ([M]$^+$ calcd for C$_{22}$H$_{21}$N: 299.17); Anal. calcd for C$_{22}$H$_{21}$N: C, 88.25; H, 7.07; N, 4.68. Found: C, 87.87; H, 7.01; N, 4.67.
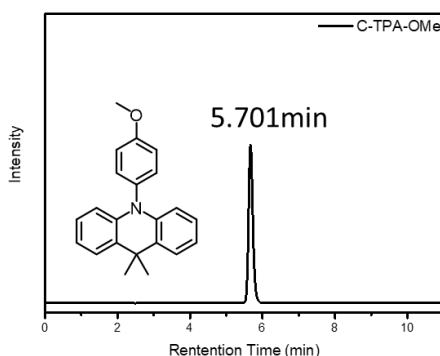
3. Additional data and spectra
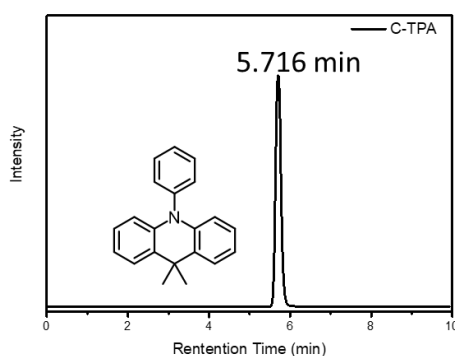
Figure S1. HPLC curve of C-TPA.

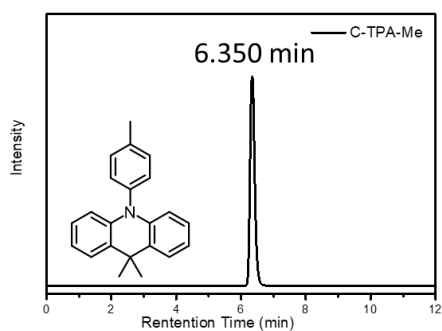**Figure S2.** HPLC curve of C-TPA-Ome.

1
2 **Figure S3.** HPLC curve of C-TPA-Me.
3
4 **Table S1.** The calculated first singlet vertical transition energy at optimized ground state geometry, and the
5 corresponding molecule orbital contribution of in gas phase.

Compound	n-th transition	E_{vert} /eV	Transition configuration (%)
C-TPA	1	3.91	H→L (13.66), H→L+1(85.56)
C-TPA-OMe	1	3.86	H→L (99.06)
C-TPA-Me	1	3.89	H→L (99.31)
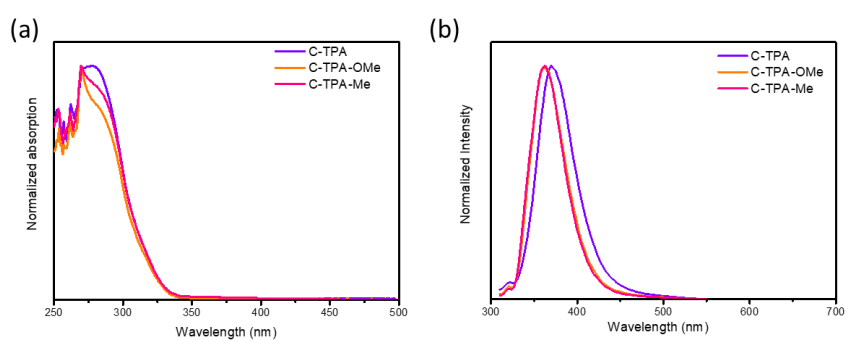
6
7 **Figure S4.** Absorption spectra(a) and PL spectra(b) of C-TPA-derivatives in THF solution with the concentration of
8 10 μM and (b) at solid state at room temperature.
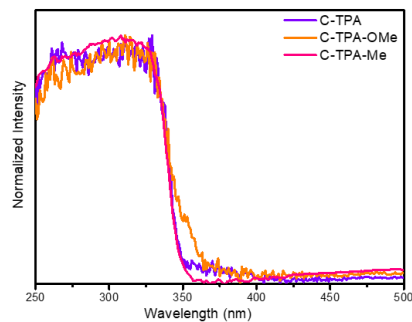
9
10 **Figure S5.** Absorption spectra of C-TPA-derivatives at solid state.
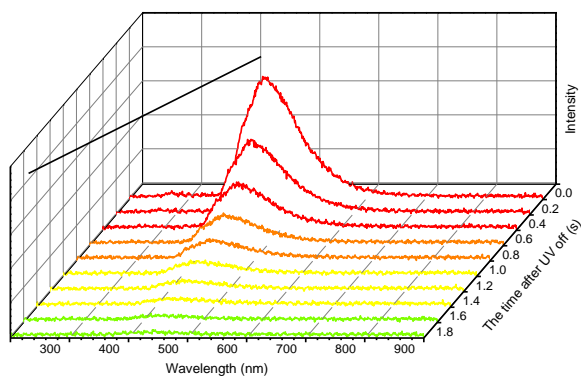11
12

4

1
2
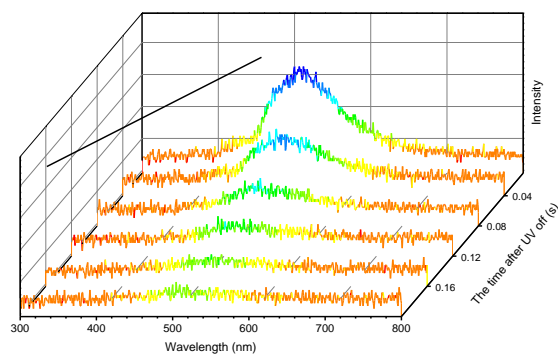
3
4 **Figure S6.** Time-dependent phosphorescence spectra of C-TPA crystal after UV excitation off at room temperature.
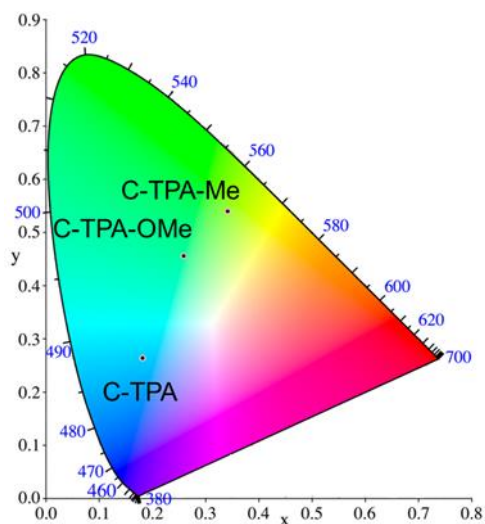
5
6
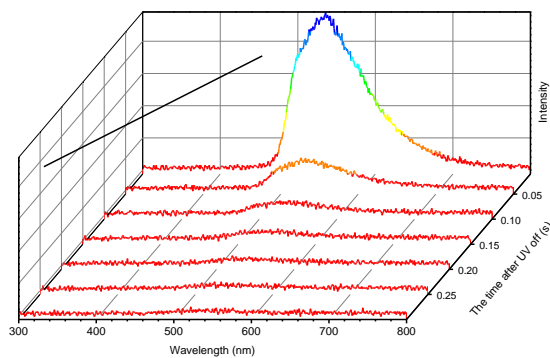
7
8 **Figure S7.** Time-dependent phosphorescence spectra of C-TPA-OMe crystal after UV excitation off at room
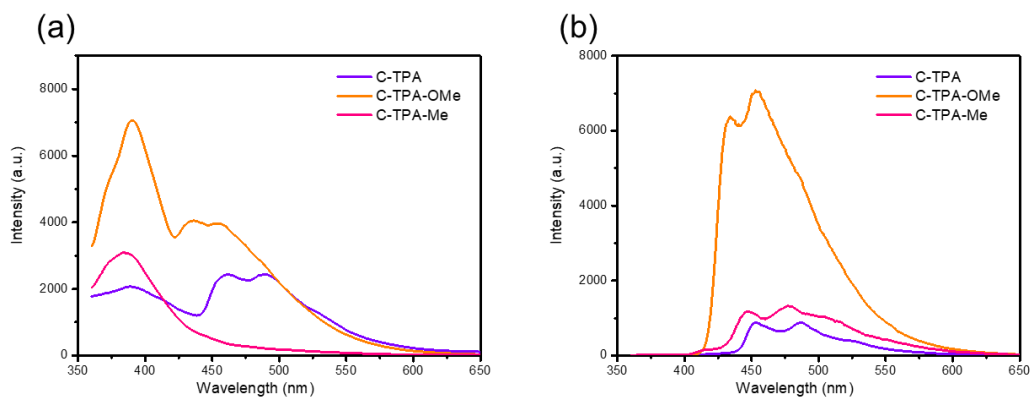9 temperature.

10

11
12 **Figure S8.** Time-dependent phosphorescence spectra of C-TPA-Me crystal after UV excitation off at room
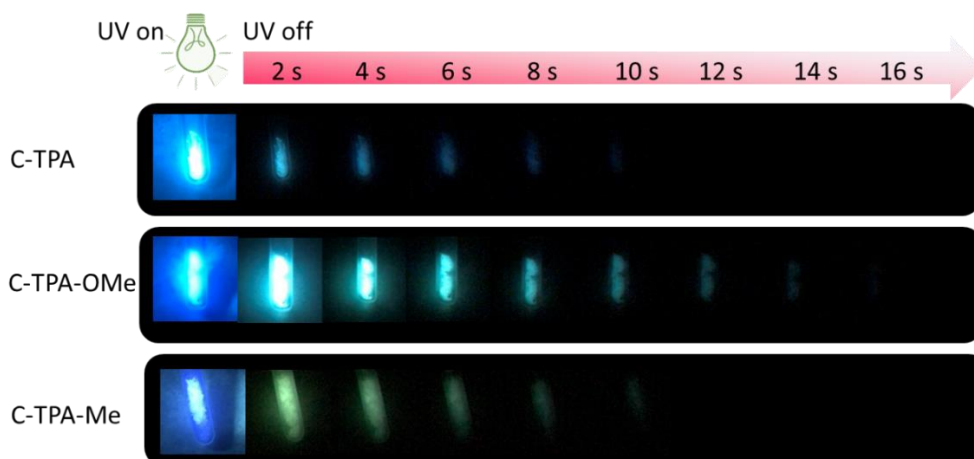13 temperature.

14

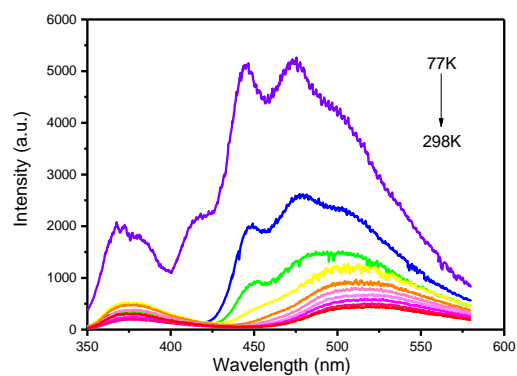**Figure S9.** Phosphorescence CIE coordinates of C-TPA-derivatives crystals.

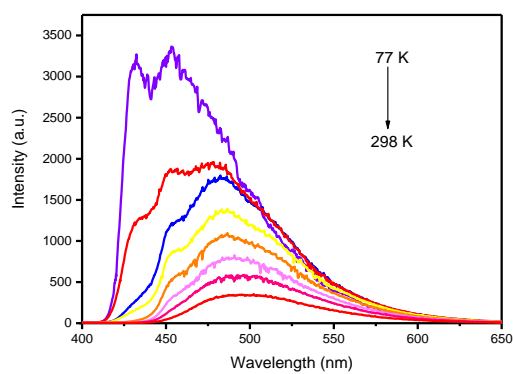**Figure S10.** PL spectra and Phosphorescence spectra of C-TPA-derivatives for crystals at 77 K.

Figure S11. The phosphorescence images for crystals of C-TPA-derivatives were taken before and after turn-off of the excitation (365 nm) at 77 K.
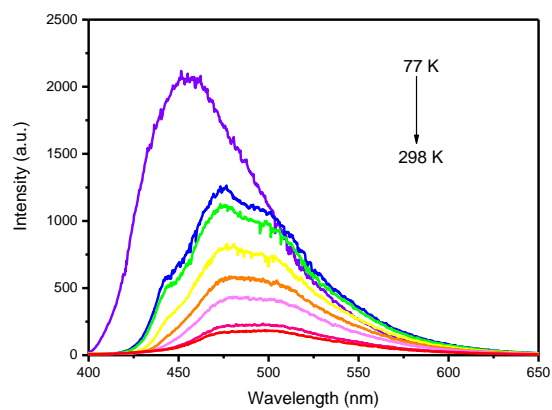
6

Figure S12. Phosphorescence spectra of C-TPA crystal at different temperature.

Figure S13. Phosphorescence spectra of C-TPA-OMe crystal at different temperatures.

Figure S14. Phosphorescence spectra of C-TPA-Me crystal at different temperatures.
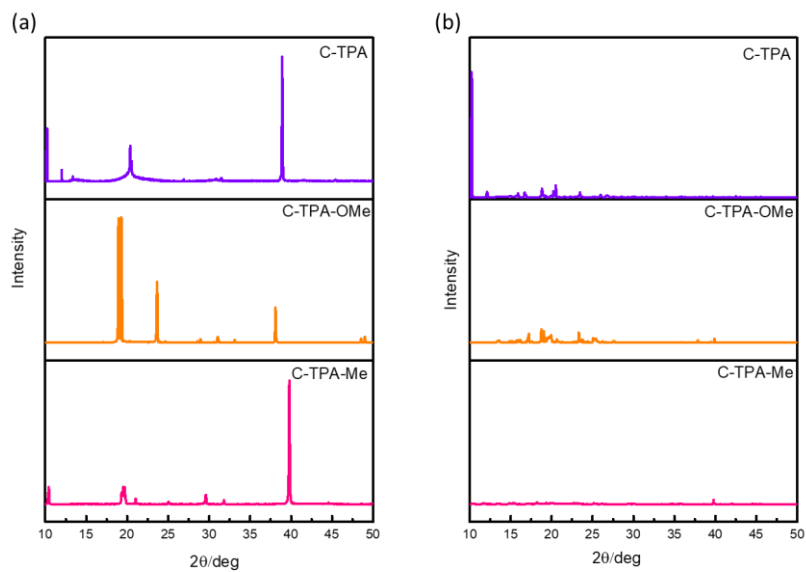
Figure S15. The XRD patterns for C-TPA-derivatives crystal(a) and powder(b).
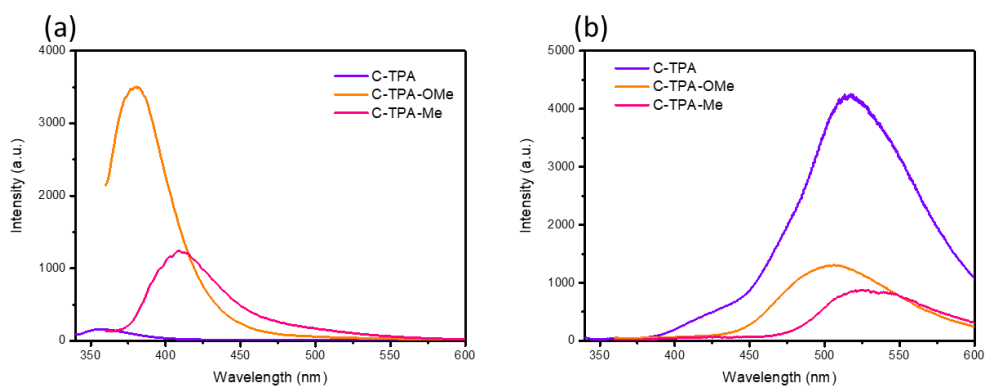

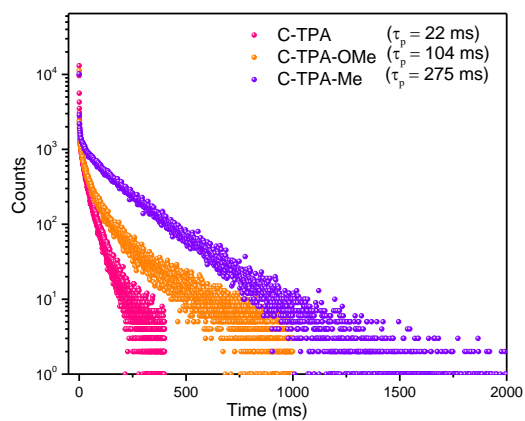Figure S16. PL spectra(a) and Phosphorescence spectra(b) of C-TPA-derivatives at powder state.

Figure S17. Phosphorescence lifetime of C-TPA-derivatives at powder state.

Table S2. Excited state energy level of monomer and dimers of three C-TPA-derivatives

Compounds	Monomer			Dimer A			Dimer B		
	S_1	T_1	ΔE_{ST}	S_1	T_1	ΔE_{ST}	S_1	T_1	ΔE_{ST}
	/eV	/eV	/eV	/eV	/eV	/eV	/eV	/eV	/eV
C-TPA	3.91	3.51	0.40	3.86	3.50	0.36	3.93	3.50	0.43
C-TPA-OMe	3.86	3.46	0.40	3.80	3.46	0.34	3.84	3.45	0.38
C-TPA-Me	3.89	3.43	0.46	3.82	3.42	0.40	3.89	3.42	0.47

C-TPA   C-TPA-OMe   C-TPA-Me
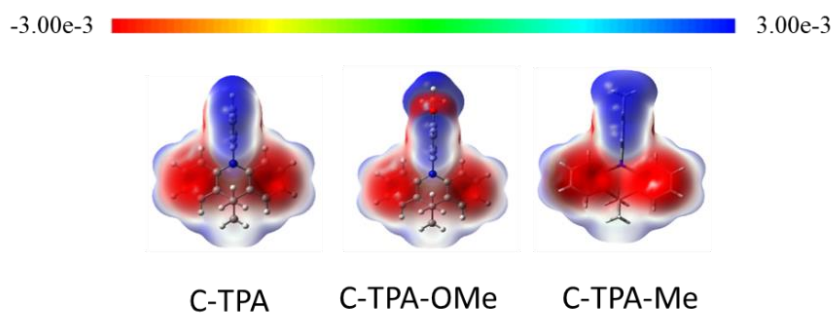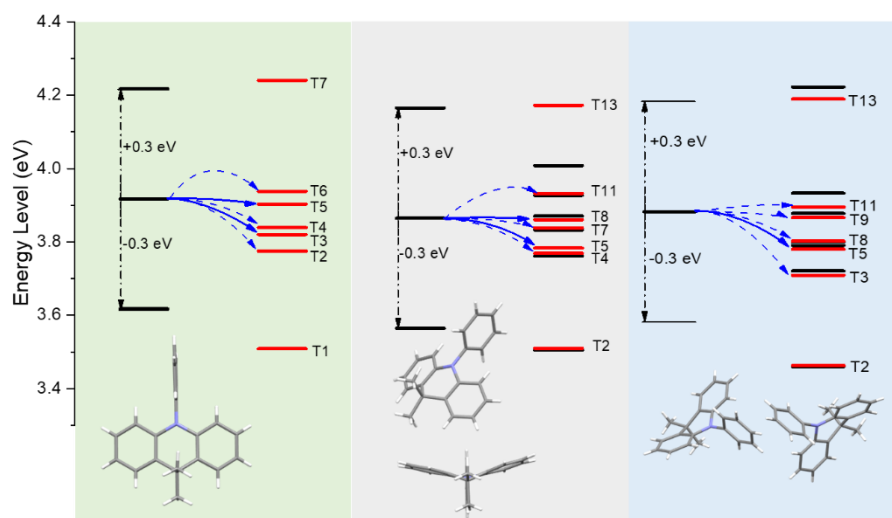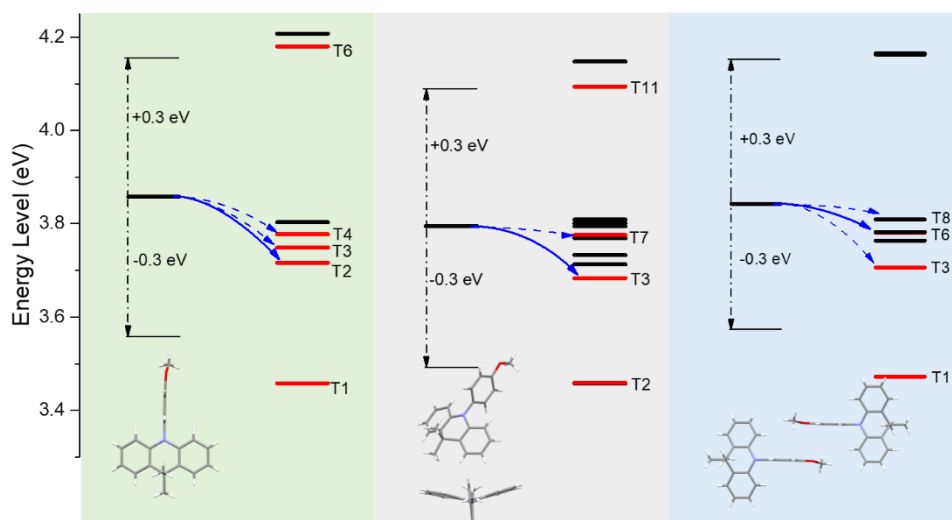
Figure S18. Difference electrostatic potential (ESP) analysis of C-TPA-derivatives as the isolated states.

Figure S19. Energy level diagrams and possible ISC channels from singlet S_1 to triplet T_n (S_0 = 0 eV) for the monomer and two types of DimerA and DimerB in C-TPA crystals. The solid arrows and dotted arrows refer to main and minor ISC channels, respectively.

Figure S20. Energy level diagrams and possible ISC channels from singlet S_1 to triplet T_n ($S_0 = 0$ eV) for the monomer and two types of DimerA and DimerB in C-TPA-OMe crystals. The solid arrows and dotted arrows refer to main and minor ISC channels, respectively.
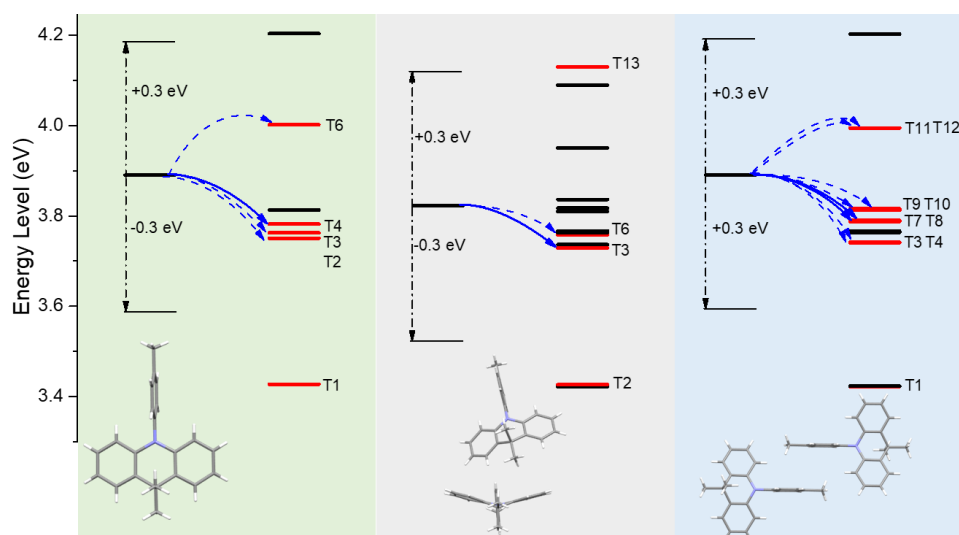

Figure S21. Energy level diagrams and possible ISC channels from singlet S_1 to triplet T_n ($S_0 = 0$ eV) for the monomer and two types of DimerA and DimerB in C-TPA-Me crystals. The solid arrows and dotted arrows refer to main and minor ISC channels, respectively.

Table S3. The matched excited state that contain the same orbital transition components of isolated TPA revealed by TD-DFT calculations.

Isolated	n-th	Energy (eV)	Transition configuration (%)
S_n	1	3.9264	H→L (97.18)
T_n	3	3.5316	H→L (95.32)

1

Table S4. The matched excited state that contain the same orbital transition components of isolated C-TPA revealed by TD-DFT calculations. The triplet state of the main ISC channel was highlighted in blue.

Isolated	n-th	Energy (eV)	Transition configuration (%)
S_n	1	3.9172	H→L (13.66), H→L+1 (85.56)
T_n	1	3.5085	H→L (8.21)
	2	3.7749	H→L (2.16)
	3	3.8199	H→L (66.83), H→L+1 (6.48)
	4	3.8392	H→L+1 (4.37)
	5	3.9029	H→L (6.04), H→L+1 (65.00)
	6	3.9378	H→L+1 (22.60)
	7	4.2401	H→L (14.83)

4

Table S5. The matched excited states that contain the same orbital transition components of dimerA of C-TPA revealed by TD-DFT calculations. The triplet state of the main ISC channel was highlighted in blue.

DimerA	n-th	Energy (eV)	Transition configuration (%)
S_n	1	3.8649	H→L+1 (12.88), H→L+3 (85.73)
T_n	2	3.5095	H→L+1 (10.20)
	4	3.7689	H→L+1 (5.24)
	5	3.7834	H→L+1 (59.22), H→L+3 (11.95)
	7	3.8381	H→L+1 (4.32), H→L+3 (20.00)
	8	3.8602	H→L+1 (5.07), H→L+3 (62.00)
	11	3.9322	H→L+1 (4.40)
	13	4.1723	H→L+1 (8.84)

7

Table S6. The matched excited states that contain the same orbital transition components of dimerB of C-TPA revealed by TD-DFT calculations. The triplet state of the main ISC channel was highlighted in blue.

DimerB	n-th	Energy (eV)	Transition configuration (%)
S_n	1	3.8649	H-1→L (16.37), H-1→L+1 (82.67)
T_n	2	3.5080	H-1→L (7.91)
	3	3.7538	H-1→L (12.69)
	5	3.8252	H→L+1 (59.22), H→L+3 (11.95)
	8	3.8475	H-1→L (17.60), H-1→L+1 (9.25)
	9	3.9119	H-1→L (6.14), H-1→L+1 (53.52)
	11	3.9402	H-1→L+1 (33.84)
	13	4.2350	H-1→L (15.08)

10
11
12
13
14
15

1

Table S7. The matched excited state that contain the same orbital transition components of isolated C-TPA-OMe revealed by TD-DFT calculations. The triplet state of the main ISC channel was highlighted in blue.

Isolated	n-th	Energy (eV)	Transition configuration (%)
S_n	1	3.8576	H→L (99.06)
T_n	1	3.4579	H→L (3.91)
	2	3.7166	H→L (46.39)
	3	3.7489	H→L (26.46)
	4	3.7771	H→L (9.16)
	6	4.1803	H→L (9.38)

4

Table S8. The matched excited states that contain the same orbital transition components of dimerA of C-TPA-OMe revealed by TD-DFT calculations. The triplet state of the main ISC channel was highlighted in blue.

DimerA	n-th	Energy (eV)	Transition configuration (%)
S_n	1	3.9032	H→L (2.64), H-1→L+1 (96.12)
T_n	2	3.4588	H-1→L+1 (4.80)
	3	3.6836	H-1→L (77.29)
	7	3.7758	H-1→ L (3.10)
	11	4.0941	H→L (95.05), H-1→L+1 (3.00)

7

Table S9. The matched excited states that contain the same orbital transition components of dimerB of C-TPA-OMe revealed by TD-DFT calculations. The triplet state of the main ISC channel was highlighted in blue.
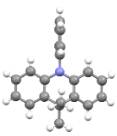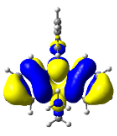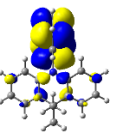
DimerB	n-th	Energy (eV)	Transition configuration (%)
S_n	1	3.8356	H→L (59.37), H-1→L+1 (39.68)
T_n	1	3.4538	H→L (2.02), H-1→L+1 (2.13)
	3	3.6947	H→L (29.63), H-1→L+1 (22.69)
	6	3.7544	H→L (12.89), H-1→L+1 (9.28)
	8	3.7731	H→L (4.54), H-1→L+1 (3.63)

10

Table S10. The matched excited state that contain the same orbital transition components of S_1 of isolated C-TPA-Me revealed by TD-DFT calculations. The triplet state of the main ISC channel was highlighted in blue.
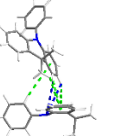
Isolated	n-th	Energy (eV)	Transition configuration (%)
S_n	1	3.8903	H→L (99.31)
T_n	1	3.4274	H→L (5.34)
	2	3.7504	H→L (5.50)
	3	3.7627	H→L (8.59)
	4	3.7820	H→L (64.13)
	6	4.0022	H→L (4.05)
	7	4.2036	H→L (11.32)

13

14

15

16

Table S11. The matched excited states that contain the same orbital transition components of dimerA of C-TPA-Me revealed by TD-DFT calculations. The triplet state of the main ISC channel was highlighted in blue.

DimerA	n-th	Energy (eV)	Transition configuration (%)
S_n	1	4.0159	H→L (73.30), H→L+1 (25.88)
T_n	2	3.7176	H→L (7.39)
	3	3.8510	H→L (50.52), H→L+1 (21.54)
	6	4.1178	H→L (5.87)
	13	4.2594	H→L (26.42), H→L+1 (70.21)
	14	4.3055	H→L (5.54), H→L+1 (2.79)

Table S12. The matched excited states that contain the same orbital transition components of dimerB of C-TPA-Me revealed by TD-DFT calculations. The triplet state of the main ISC channel was highlighted in blue.
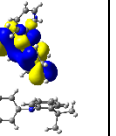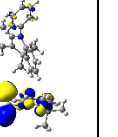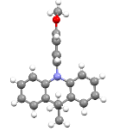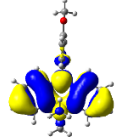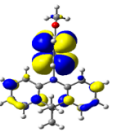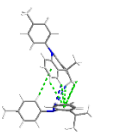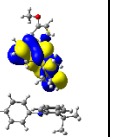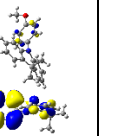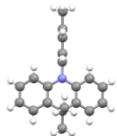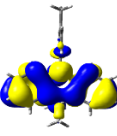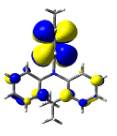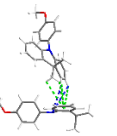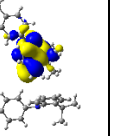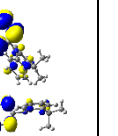
DimerB	n-th	Energy (eV)	Transition configuration (%)
S_n	1	3.8649	H-1→L (12.72), H-1→L+1 (11.68), H→L (45.30), H→L+1 (26.21)
T_n	3	3.7411	H-1→L (3.73), H-1→L+1 (4.53), H→L+1 (7.24)
	4	3.7416	H-1→L+1 (6.94), H→L (4.17), H→L+1 (4.07)
	7	3.7879	H-1→L (6.23), H-1→L+1 (9.03), H→L (29.43), H→L+1 (15.72)
	8	3.7902	H-1→L (27.09), H-1→L+1 (16.67), H→L (5.53), H→L+1 (9.53)
	9	3.8124	H→L+1 (2.36)
	10	3.8158	H-1→L+1 (2.84)
	11	3.9946	H-1→L (10.59), H→L (12.73), H→L+1 (6.01)
	12	3.9948	H-1→L (13.54), H-1→L+1 (5.22), H→L (10.85)

Table S13. The molecular conformations and HOMO, LUMO orbits for the isolated molecules and coupled units of C-TPA, C-TPA-OMe, C-TPA-Me.

	Monomer	HOMO	LUMO	Dimer	HOMO	LUMO
C-TPA						
C-TPA-OMe						
C-TPA-Me						

1
2
3 **Table S14.** The NTO of singlet and triplet state of the main ISC channel for the isolated molecules of TPA, C-TPA, C-
4 TPA-Me, C-TPA-OMe.

| Sample		Hole	Partical		Hole	Partical
TPA	S1			T1		
				T3		
C-TPA	S1			T1		
				T3		
				T5		
C-TPA-OMe	S1			T1		
				T2		
				T3		
C-TPA-Me	S1			T1		
				T2		
				T3		

5
6
7
8
9
10

14

1

2

Table S15. Structure data of single crystals of **C-TPA, C-TPA-Me** and **C-TPA-OMe**.

Name	C-TPA	C-TPA-OMe	C-TPA-Me
Formula	$C_{21}H_{19}N$	$C_{22}H_{21}NO$	$C_{22}H_{21}N$
Crystal system	monoclinic	monoclinic	monoclinic
Space Group	P 1 21/n 1	P 1 21/n 1	P 1 21/c 1
Cell Lengths (Å)	11.566(3) 8.165(2) 17.398(5)	11.852(9) 8.143(6) 17.994(14)	9.385(2) 22.876(6) 8.232(2)
Cell Angles (o)	90 101.917(5) 90	90 96.816(12) 90	90 105.446(3) 90
Cell Volume ($Å^3$)	1607.5(8)	1724(2)	1703.6(7)
Z	4	4	4
Density (g/cm^3)	1.179	1.215	1.167
CCDC Number	2081904	2081906	2081905

3

4
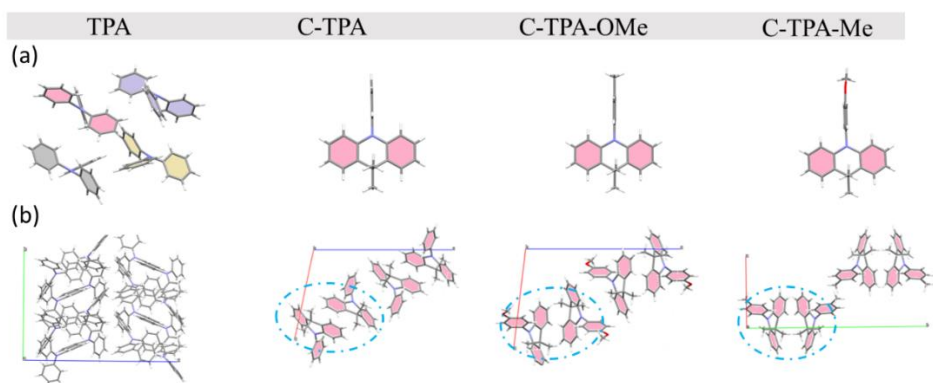
5 **Figure S22.** Single-crystal structures of the TPA and three target compounds. (a) monomer (b) unit cell.

6

7

8

Table S16. The intermolecular interactions of dimerA and dimerB in C-TPA-derivatives crystals.

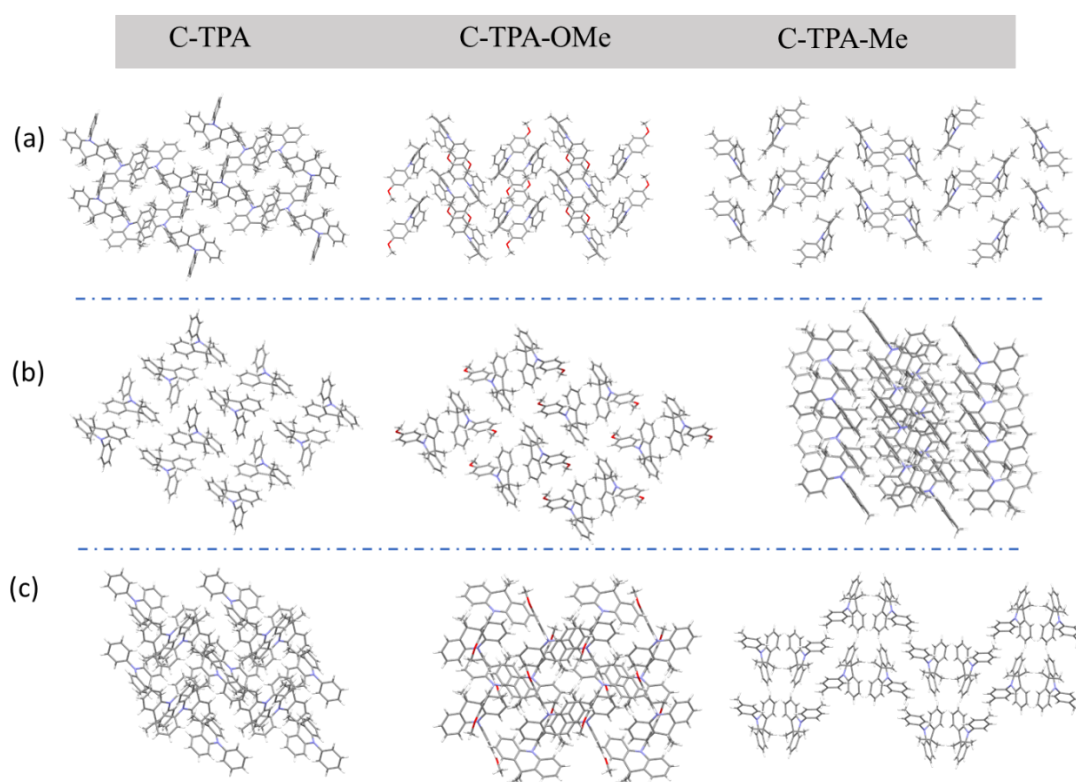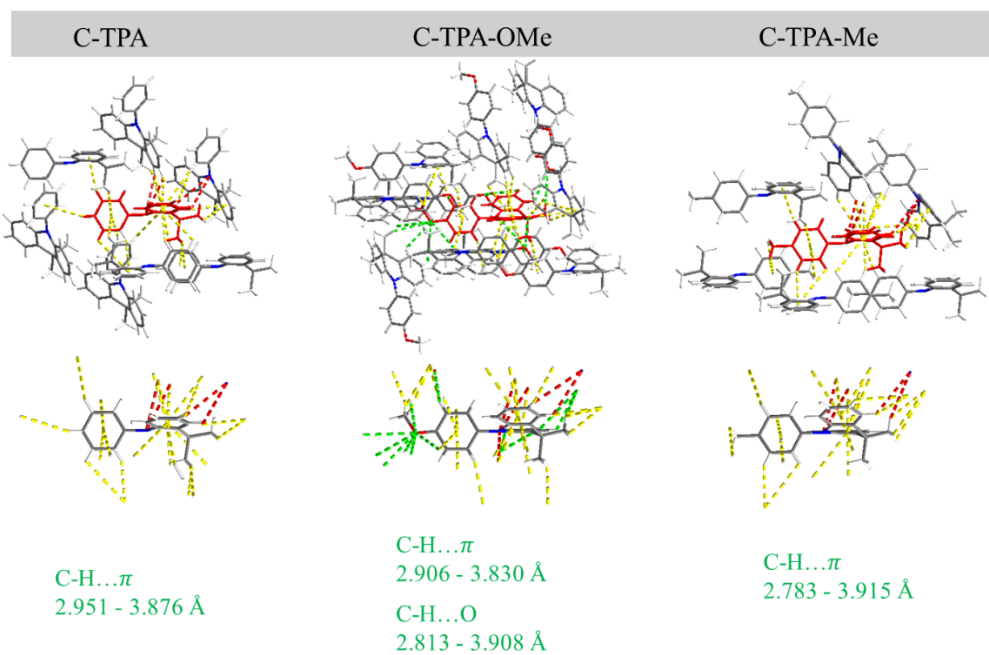| Sample	Dimer A		Dimer B	
	C-H…π	C-H…N:	C-H…π:	C-H…X:
C-TPA	2.983 Å, 3.040 Å, 3.505 Å, 3.770 Å	3.450 Å 3.632 Å	3.328 Å, 3.743 Å	0
C-TPA-OMe	2.905 Å, 3.279 Å 3.284 Å, 3.830 Å	3.598 Å 3.909 Å	3.554 Å 3.554 Å	3.875 Å, 3.875 Å
C-TPA-Me	2.800 Å, 3.246 Å, 3.480 Å, 3.664 Å, 3.675 Å,3.694 Å	3.556 Å 3.898 Å	3.915 Å, 3.749 Å, 3.915 Å, 3.749 Å	0

Figure S23. The Molecular packing of C-TPA, C-TPA-OMe and C-TPA-Me, crystal observed from the (a)a axial, (b)b axial, and (c)c axial directions, respectively.

1
2

| C-TPA | C-TPA-OMe | C-TPA-Me |

C-H…π
2.951 - 3.876 Å

C-H…π
2.906 - 3.830 Å

C-H…O
2.813 - 3.908 Å

C-H…π
2.783 - 3.915 Å

3

4   **Figure S24.** Dimers and intermolecular interactions in crystal C-TPA, C-TPA-OMe and C-TPA-Me.

5

UV on   UV off
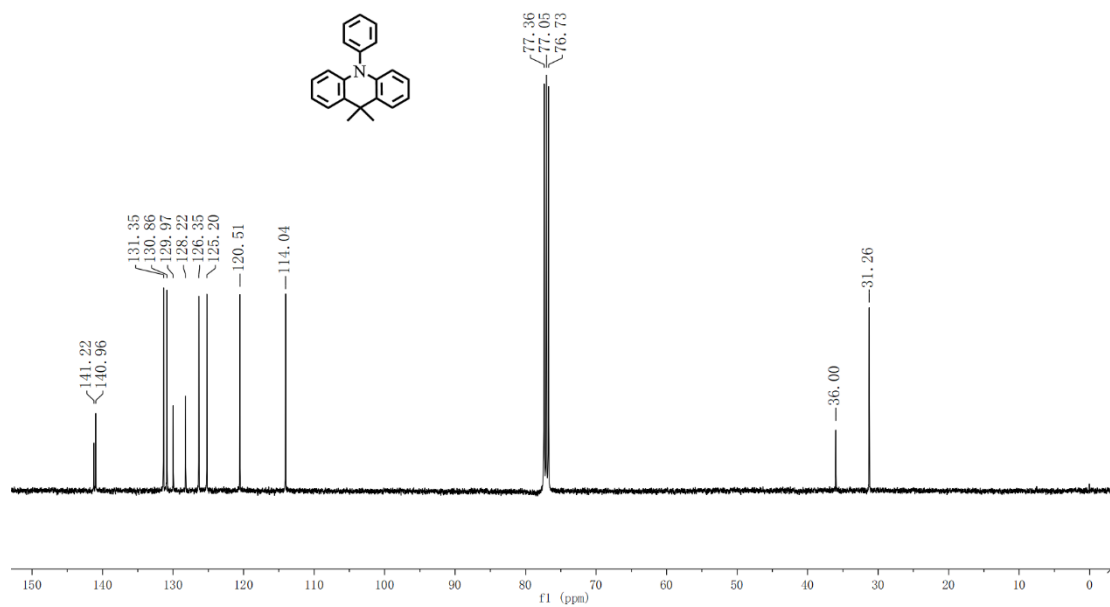
0.5s   1.5s

6
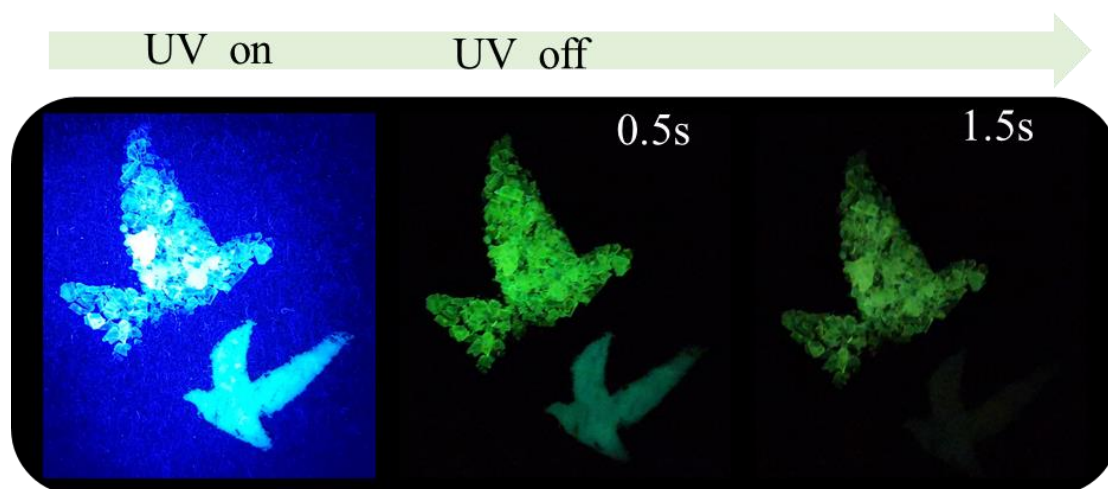
7   **Figure S25.** Various patterns constructed by C-TPA-derivatives. bird(up) used by C-TPA-Me and bird(bottom) used

8   by C-TPA, the patterns of emission before and after UV irradiation.

9
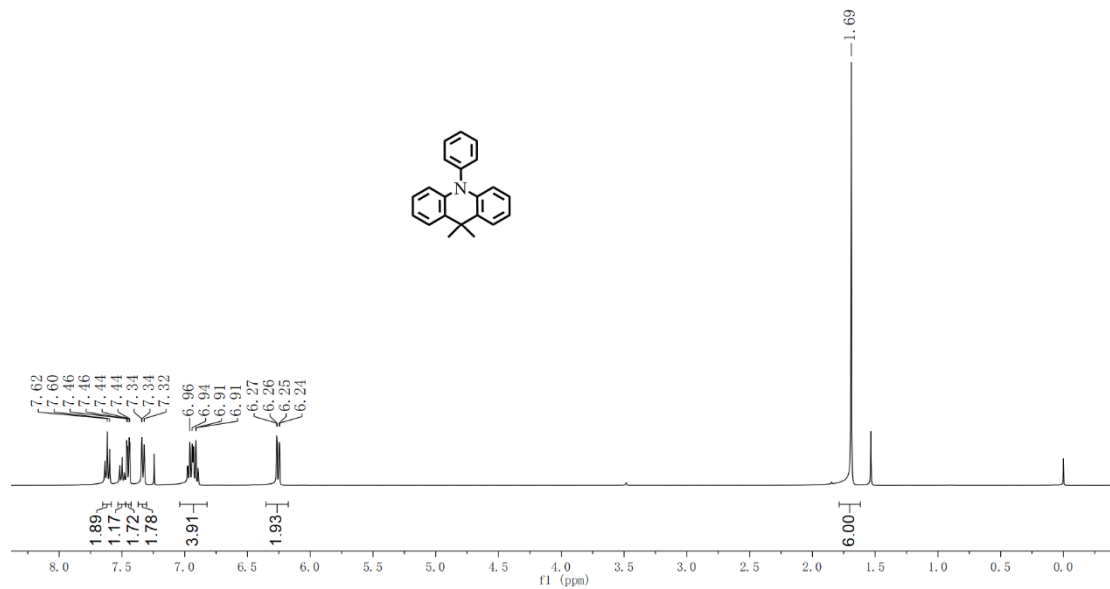
Figure S26. ^{1}H NMR spectrum of C-TPA (in CDCl$_3$).

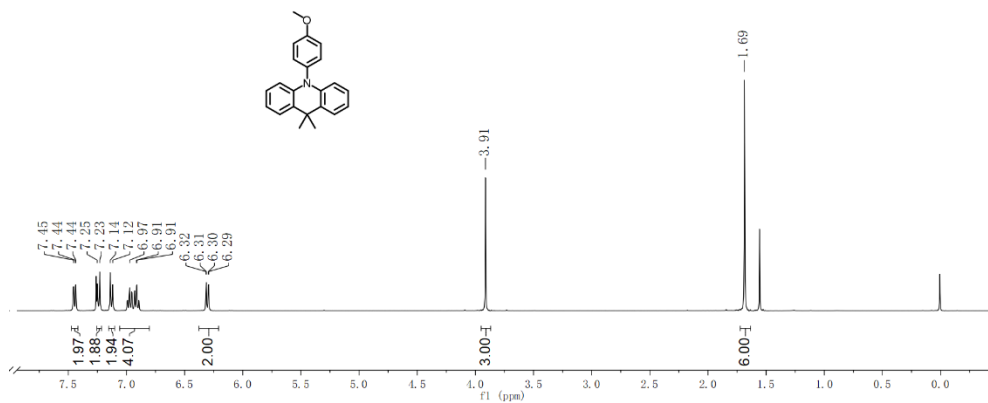**Figure S27.** ^{13}C NMR spectrum of C-TPA (in CDCl$_3$).
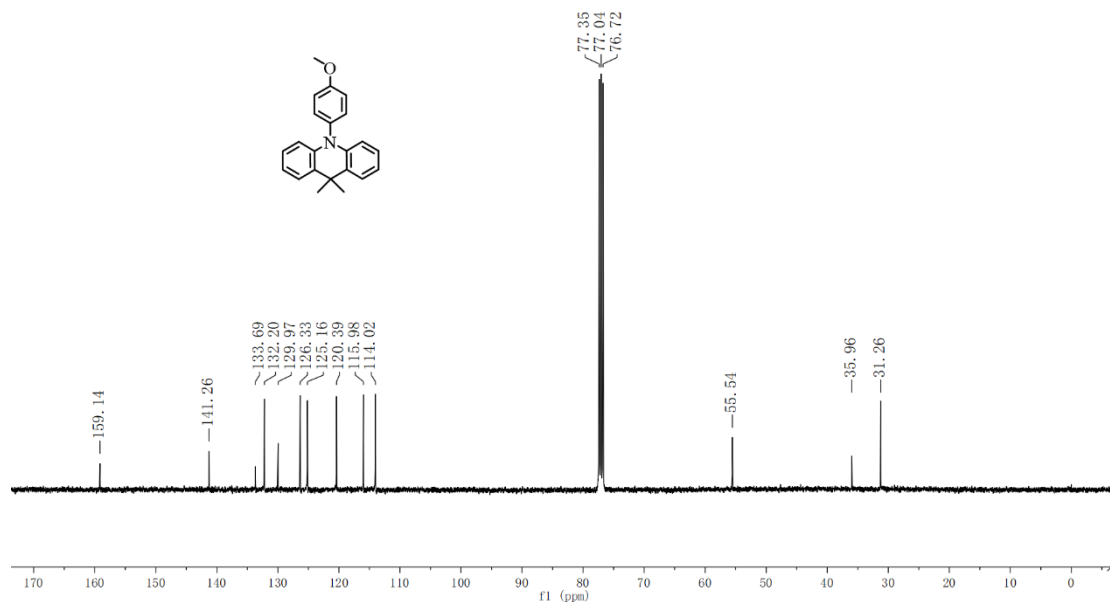
Figure S28. ¹H NMR spectrum of C-TPA-OMe (in CDCl₃).

Figure S29. ¹³C NMR spectrum of C-TPA-OMe (in CDCl₃).

1

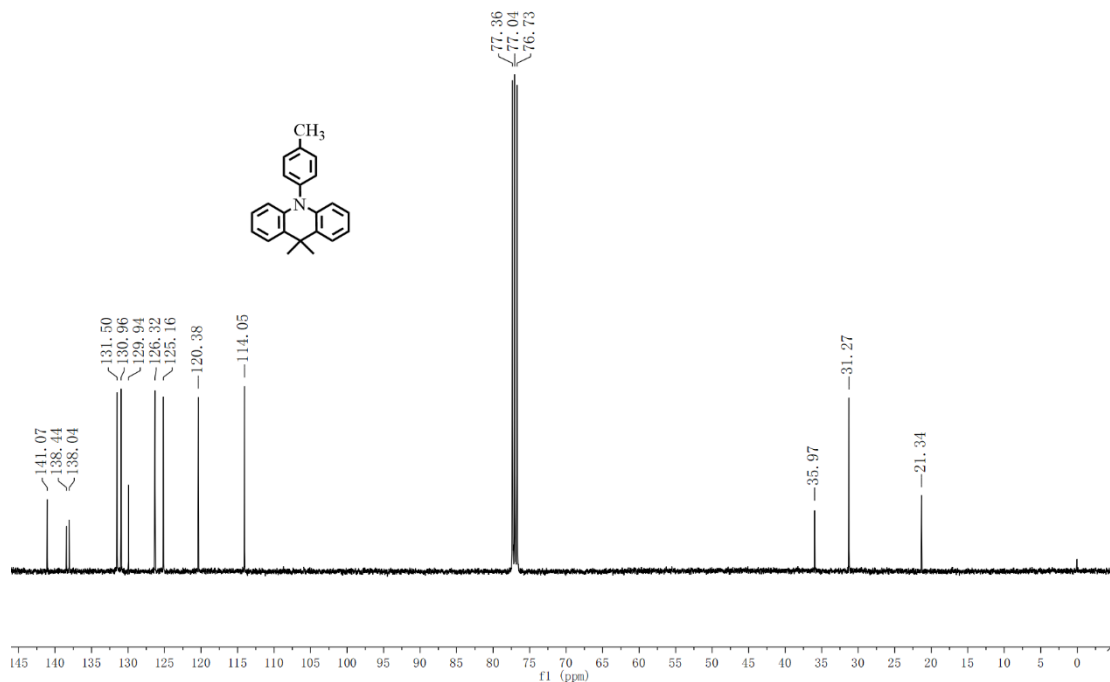2   **Figure S30**. ^{1}H NMR spectrum of C-TPA-Me (in CDCl$_3$).

3

4   **Figure S31**. ^{13}C NMR spectrum of C-TPA-Me (in CDCl$_3$).

5

6   **Reference**

7   1.   Gaussian 09, Revision D.01, M. J. Frisch, G. W. Trucks, H. B. Schlegel, G. E. Scuseria, M. A. Robb, J. R.

8   Cheeseman, G. Scalmani, V. Barone, B. Mennucci, G. A. Petersson, H. Nakatsuji, M. Caricato, X. Li, H. P.

1   Hratchian, A. F. Izmaylov, J. Bloino, G. Zheng, J. L. Sonnenberg, M. Hada, M. Ehara, K. Toyota, R. Fukuda, J.

2   Hasegawa, M. Ishida, T. Nakajima, Y. Honda, O. Kitao, H. Nakai, T. Vreven, J. A. Montgomery, Jr., J. E. Peralta,

3   F. Ogliaro, M. Bearpark, J. J. Heyd, E. Brothers, K. N. Kudin, V. N. Staroverov, T. Keith, R. Kobayashi, J.

4   Normand, K. Raghavachari, A. Rendell, J. C. Burant, S. S. Iyengar, J. Tomasi, M. Cossi, N. Rega, J. M. Millam,

5   M. Klene, J. E. Knox, J. B. Cross, V. Bakken, C. Adamo, J. Jaramillo, R. Gomperts, R. E. Stratmann, O. Yazyev, A.

6   J. Austin, R. Cammi, C. Pomelli, J. W. Ochterski, R. L. Martin, K. Morokuma, V. G. Zakrzewski, G. A. Voth, P.

7   Salvador, J. J. Dannenberg, S. Dapprich, A. D. Daniels, O. Farkas, J. B. Foresman, J. V. Ortiz, J. Cioslowski, and

8   D. J. Fox, Gaussian, Inc., Wallingford CT, 2013.

9   2.   T. Lu, F. Chen, Multiwfn: A multifunctional wavefunction analyzer, *J. Comput. Chem.* 2012, 33, 580.